PAPER • OPEN ACCESS

High-resolution spectroscopy of gaseous ^{83m}Kr conversion electrons with the KATRIN experiment

View the article online for updates and enhancements.
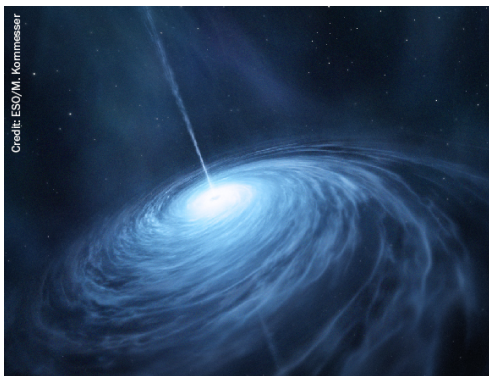
High-resolution spectroscopy of gaseous [83m]Kr conversion electrons with the KATRIN experiment

K Altenmüller[1,2], M Arenz[3], W-J Baek[4], M Beck[5],
A Beglarian[6], J Behrens[4], T Bergmann[6], A Berlev[7],
U Besserer[8], K Blaum[9], F Block[4], S Bobien[8], T Bode[1,10],
B Bornschein[8], L Bornschein[11], T Brunst[1,10], N Buzinsky[12],
S Chilingaryan[6], W Q Choi[4], M Deffert[4], P J Doe[13],
O Dragoun[14], G Drexlin[4], S Dyba[15], F Edzards[1,10], K Eitel[11],
E Ellinger[16], R Engel[11], S Enomoto[13], D Eversheim[3],
M Fedkevych[15], J A Formaggio[12], F M Fränkle[11],
G B Franklin[17], F Friedel[4], A Fulst[15], W Gil[11], F Glück[11],
A Gonzalez Ureña[18], S Grohmann[8], R Grössle[8],
R Gumbsheimer[11], M Hackenjos[4,8], V Hannen[15], F Harms[4],
N Haußmann[16], F Heizmann[4], K Helbing[16], S Hickford[4,16],
D Hilk[4], D Hillesheimer[8], D Hinz[4], M A Howe[19,20], A Huber[4],
A Jansen[11], J Kellerer[4], N Kernert[11], L Kippenbrock[13],
M Klein[4], A Kopmann[6], M Korzeczek[4], A Kovalík[14],
B Krasch[8], M Kraus[4], T Lasserre[1,2], O Lebeda[14], J Letnev[21],
A Lokhov[7], M Machatschek[4], A Marsteller[8], E L Martin[13,19],
S Mertens[1,10], S Mirz[8], B Monreal[22], H Neumann[8],
S Niemes[8], A Off[8], A Osipowicz[21], E Otten[5], D S Parno[17],
P Plischke[11], A Pollithy[1,10], A W P Poon[23], F Priester[8],
P C-O Ranitzsch[15], O Rest[15], R G H Robertson[13],
F Roccati[10,11], C Rodenbeck[15], M Röllig[8], C Röttele[4],
M Ryšavý[14], R Sack[15], A Saenz[24], L Schimpf[4],
K Schlösser[11], M Schlösser[8], K Schönung[9], M Schrank[11],
H Seitz-Moskaliuk[4], J Sentkerestiová[14], V Sibille[12], M
Slezák[10,26], M Steidl[11], N Steinbrink[15], M Sturm[8],
M Suchopar[14], M Suesser[8], H H Telle[18], L A Thorne[17],
T Thümmler[11], N Titov[7], I Tkachev[7], N Trost[11], K Valerius[11],
D Vénos[14], R Vianden[3], A P Vizcaya Hernández[17], M Weber[6],
C Weinheimer[15], S Welte[8], J Wendel[8], J F Wilkerson[19,20,25],
J Wolf[4], S Wüstling[6], S Zadoroghny[7] and G Zeller[8]

[1] Technische Universität München, James-Franck-Str. 1, 85748 Garching, Germany
[2] IRFU, CEA, Université Paris-Saclay, 91191 Gif-sur-Yvette, France
[3] Helmholtz-Institut für Strahlen- und Kernphysik, Rheinische Friedrich-Wilhelms Universität Bonn, Nussallee 14-16, 53115 Bonn, Germany
[4] Karlsruhe Institute of Technology (KIT), Institute of Experimental Particle Physics (ETP), Wolfgang-Gaede-Str. 1, 76131 Karlsruhe, Germany
[5] Institut für Physik, Johannes-Gutenberg-Universität Mainz, 55099 Mainz, Germany
[6] Karlsruhe Institute of Technology (KIT), Institute for Data Processing and Electronics (IPE), Postfach 3640, 76021 Karlsruhe, Germany
[7] Institute for Nuclear Research of Russian Academy of Sciences, 60th October Anniversary Prospect 7a, 117312 Moscow, Russia
[8] Karlsruhe Institute of Technology (KIT), Institute for Technical Physics (ITeP), Postfach 3640, 76021 Karlsruhe, Germany
[9] Max-Planck-Institut für Kernphysik, Saupfercheckweg 1, 69117 Heidelberg, Germany
[10] Max-Planck-Institut für Physik, Föhringer Ring 6, 80805 München, Germany
[11] Karlsruhe Institute of Technology (KIT), Institute for Nuclear Physics (IKP), Postfach 3640, 76021 Karlsruhe, Germany
[12] Laboratory for Nuclear Science, Massachusetts Institute of Technology, 77 Massachusetts Ave, Cambridge, MA 02139, United States of America
[13] Center for Experimental Nuclear Physics and Astrophysics, and Dept. of Physics, University of Washington, Seattle, WA 98195, United States of America
[14] Nuclear Physics Institute of the CAS, v. v. i., CZ-250 68 Řež, Czech Republic
[15] Institut für Kernphysik, Westfälische Wilhelms-Universität Münster, Wilhelm-Klemm-Str. 9, 48149 Münster, Germany
[16] Department of Physics, Faculty of Mathematics und Natural Sciences, University of Wuppertal, Gauss-Str. 20, 42119 Wuppertal, Germany
[17] Department of Physics, Carnegie Mellon University, Pittsburgh, PA 15213, United States of America
[18] Universidad Complutense de Madrid, Instituto Pluridisciplinar, Paseo Juan XXIII, nº 1, 28040 - Madrid, Spain
[19] Department of Physics and Astronomy, University of North Carolina, Chapel Hill, NC 27599, United States of America
[20] Triangle Universities Nuclear Laboratory, Durham, NC 27708, United States of America
[21] University of Applied Sciences (HFD) Fulda, Leipziger Str. 123, 36037 Fulda, Germany
[22] Department of Physics, Case Western Reserve University, Cleveland, OH 44106, United States of America
[23] Institute for Nuclear and Particle Astrophysics and Nuclear Science Division, Lawrence Berkeley National Laboratory, Berkeley, CA 94720, United States of America
[24] Institut für Physik, Humboldt-Universität zu Berlin, Newtonstr. 15, 12489 Berlin, Germany

E-mail: slezak@mpp.mpg.de

CrossMark

[25] Also affiliated with Oak Ridge National Laboratory, Oak Ridge, TN 37831, United States of America.

[26] Author to whom any correspondence should be addressed.

Abstract

In this work, we present the first spectroscopic measurements of conversion electrons originating from the decay of metastable gaseous [83m]Kr with the Karlsruhe Tritium Neutrino (KATRIN) experiment. The obtained results represent one of the major commissioning milestones for the subsequent direct neutrino mass measurement with KATRIN. The successful campaign demonstrates the functionalities of the KATRIN beamline. Precise measurement of the narrow K-32, L_3-32, and $N_{2,3}$-32 conversion electron lines allowed to verify the eV-scale energy resolution of the KATRIN main spectrometer necessary for competitive measurement of the absolute neutrino mass scale.

Keywords: neutrino mass, electrostatic spectrometer, calibration, conversion electrons

(Some figures may appear in colour only in the online journal)

1. Introduction

The results obtained in neutrino oscillation experiments have shown conclusively that neutrinos are massive particles [1–3]. As oscillations provide only information on the differences of the mass eigenvalues squared (Δm^2), the absolute neutrino mass scale has to be addressed by other means. Complementary results related to the absolute neutrino mass scale are provided by cosmological observations [4, 5], neutrinoless double β-decay searches [6–8], and direct measurements that utilize β-decays [9–12]. The direct measurements do not require any assumptions of the neutrino nature or mass model, and rely solely on kinematic considerations. As pointed out by Fermi in 1934 [13], a non-zero neutrino mass manifests itself as a distortion near the endpoint region of the β-electron energy spectrum. While the experimental energy resolution is not good enough to resolve individual neutrino mass states, the observable extracted from the β-spectrum is the effective electron (anti)-neutrino mass squared. It is an incoherent superposition of the mass eigenvalues, $m_\beta^2 = \sum_i |U_{ei}|^2 m_i^2$, where U_{ei} are the Pontecorvo–Maki–Nakagawa–Sakata mixing matrix elements [14].

A particularly suitable isotope for direct neutrino mass measurement is tritium due to its low endpoint energy of about 18.6 keV and favorable decay properties (super-allowed $1/2^+ \rightarrow 1/2^+$ transition). As of today, only upper limits on m_β have been obtained; up to recently the most stringent limits came from the tritium experiments in Mainz with $m_\beta < 2.3 \, \text{eV}/c^2$ (95% C.L.) [15] and Troitsk with $m_\beta < 2.05 \, \text{eV}/c^2$ (95% C.L.) [16], respectively. The KATRIN (KArlsruhe TRItium Neutrino) experiment is a next-generation tritium β-decay experiment designed to search for m_β with a sensitivity of $0.2 \, \text{eV}/c^2$ (90% C.L.) and a 5σ discovery potential of $m_\beta = 0.35 \, \text{eV}/c^2$ [9]. It utilizes a highly luminous windowless gaseous tritium source and an electrostatic spectrometer with high resolution and large angular acceptance. The results reported in the present paper were used to ensure the readiness of the first physics results of KATRIN that yielded a new upper limit of $m_\beta < 1.1 \, \text{eV}/c^2$ (90% C.L.) [17].

The metastable isotope [83m]Kr, with monoenergetic conversion electrons close to the tritium β-endpoint energy and additional electrons up to 32 keV [18, 19], has served in the past as a vital calibration and commissioning source for tritium-based direct neutrino-mass measurements [20–22]. The isotope has a short half-life of 1.83 h and, as a noble gas with no long-lived daughters, can be allowed to diffuse through the experimental apparatus without the risk of long-term radioactive contamination. These characteristics give [83m]Kr broad

utility as a calibration source in gaseous and liquid detectors. For example, ^{83m}Kr electrons have been used for more than 25 years to calibrate time projection chambers and calorimeters in high-energy particle physics, operating in a variety of gas mixtures: Xe/CO$_2$ [23, 24], Ar/CH$_4$ [25], Ar/CH$_4$/CO$_2$ and Ne/CO$_2$ [26]. ^{83m}Kr is also a widely used calibration source for direct dark-matter searches using noble-gas detectors, which require excellent characterization at low energies [27–31] and a robust understanding of the gas system [32].

The natural widths of the ^{83m}Kr electron lines are of eV scale, comparable to the resolution required for competitive direct neutrino-mass measurements. The project 8 experiment, aiming to use cyclotron radiation emission spectroscopy on tritium β-decay [33], reported on the first measurements of these lines in [34]. In this paper, we report on the results of gaseous ^{83m}Kr conversion electron measurements performed with the KATRIN β-beamline during the pre-tritium commissioning phase. The measurements allowed us to assess the performance of the practically complete KATRIN setup (see section 2 below) over a broad energy range using the sharp lines of the ^{83m}Kr conversion electrons, characterized by different linewidths. We have obtained high-resolution spectra of conversion electron lines at the energies of 17.8 keV, 30.5 keV and 32.1 keV, extracting line widths and positions by means of a maximum likelihood analysis. Earlier reports on the line widths [35, 36] used a condensed source for the measurements which may be subject to a possible broadening of the lines due to surface effects. According to [35], the ^{83m}Kr atoms were deposited at different distances from the substrate and thus experienced different mirror charges leading effectively to a broadening. The broadening was described in a generic way by convolving the electron line shape with a Gaussian function whose width served as an additional unconstrained free parameter in the analysis. In [37], generic uncertainty estimates of the recommended line widths are given for different levels and regions of the atomic number Z. For $Z = 36$, the atomic number of ^{83m}Kr, ranges of 5%–10% for the K shell and 10%–30% for the L$_3$ subshell, respectively, are suggested. In this work the systematic uncertainties are treated comprehensively and quantitatively for the first time.

2. The KATRIN experiment

The KATRIN electron spectrometer operates as an integrating electrostatic filter with magnetic adiabatic collimation (MAC-E filter) [21, 38]. During neutrino mass measurements, electrons are delivered via β-decays of molecular tritium in the windowless gaseous tritium source (WGTS) [39]. To prevent tritium from reaching the MAC-E filter where it would cause elevated background, differential (DPS) and cryogenic pumping sections (CPS), together forming the electron transport section, are installed between the WGTS and the spectrometer [40, 41]. Electrons with sufficient kinetic energy are transmitted through the pre- and main spectrometers and are eventually counted by a 148-segmented Si PIN-diode—the focal plane detector (FPD) [42]. The MAC-E filter spectroscopy technique was successfully applied at previous direct neutrino mass experiments in Mainz [15] and Troitsk [16]. Gaseous tritium sources were used in the Los Alamos National Laboratory experiment [20] and in Troitsk [16]. For a detailed overview of the technical aspects of the KATRIN apparatus, the reader is referred to [40].

In the KATRIN experiment, ^{83}Rb/^{83m}Kr source (in the following indicated as ^{83m}Kr source) is applied in three forms: gaseous, condensed, and implanted. Their common attribute is the continuous generation of ^{83m}Kr from electron capture decay of its parent radionuclide ^{83}Rb, which has a half-life of 86.2 d. The parent half-life ensures a continuous supply of the short-lived ^{83m}Kr necessary for spectroscopy measurements with the MAC-E filter. In all cases, physical, chemical, or mechanical means are deployed to ensure that the ^{83}Rb itself does not leave its housing. For example, in the case of gaseous ^{83m}Kr source, the ^{83}Rb is deposited in

zeolite (molecular sieve) [43] and stored in a dedicated generator setup [44]. To prevent spreading of eventual [83]Rb-loaded zeolite debris, the setup features two sintered metal filters with a pore size of 0.5 μm. Thus, only [83m]Kr is released and any electron emitted after the [83]Rb decay does not influence the measurements of [83m]Kr conversion electrons. A description of the other sources can be found in [40].

In this paper, we focus on the analysis of the measurements obtained with the gaseous [83m]Kr source (GKrS). The basic principle of the GKrS is to introduce gaseous [83m]Kr into the WGTS. Similar to tritium, it behaves as a spatially distributed isotropic source of electrons, which allows for testing of the entire KATRIN setup in the same configuration as that during the neutrino mass measurement. Even more importantly, as [83m]Kr and tritium can share the common volume in the source beam tube, the GKrS will allow us to study space-charge effects in the tritium plasma contributing to the source potential. Unaccounted potential variations within the source would effectively smear out the tritium β-spectrum, leading to a systematic shift of the observed m_β^2 [45]. The only difference to standard tritium operation is the higher WGTS beam tube temperature of $T = 100$ K, instead of the default 30 K (achieved using a dual-phase bath with argon instead of neon [40]). This change prevents the freeze-out of [83m]Kr on the beam-tube walls. The use of [83m]Kr in a gaseous source for space charge investigation was reported by the Troitsk group [46]. In this [83m]Kr measurement a part of the KATRIN setup, the rear section (RS) which is equipped with an electron gun and a gold-plated rear wall, was not available. Instead, a stainless steel flange terminated the beamline at the end of the WGTS. The measurement was performed without an additional carrier gas inside the source section resulting in a negligible column density compared to tritium operation. In contrast with the KATRIN final design of the circulating [83m]Kr gas, the gas was left to propagate freely in the vacuum from the generator into the beam tube and was pumped only by the cold inner surface of the CPS.

3. Measurements

The energy of the conversion electron—emitted from a particular subshell of the [83m]Kr atom inside the WGTS—with respect to the beam tube vacuum level is [19]

$$E = E_\gamma + E_{\gamma,\,\text{rec}} - E_{\text{e, rec}} - E_{\text{e, bin}}, \tag{1}$$

where E_γ is the energy of the corresponding gamma ray, $E_{\gamma,\text{rec}}$ is the recoil energy after gamma-ray emission, $E_{\text{e,rec}}$ is the recoil energy after electron emission, and $E_{\text{e,bin}}$ is the electron atomic binding energy. To analyze the electron energy, the spectrometer is biased with respect to the grounded source tube by a negative retarding voltage U thus creating an electrostatic barrier. The electron passes the barrier when its energy E is equal to or larger than the spectrometer vacuum level. Denoting the source and spectrometer work functions as Φ_{src} and Φ_{spec}, respectively, the transmission condition is

$$E \geqslant qU - (\Phi_{\text{src}} - \Phi_{\text{spec}}), \tag{2}$$

where $q < 0$ is the electron charge and qU is the retarding energy. Thus, the MAC-E filter measures an effective electron energy qU that appears to be shifted from the expected kinetic energy E by the work-function difference $\Phi_{\text{src}} - \Phi_{\text{spec}}$.

The MAC-E filter has a finite energy resolution ΔE, which is defined for adiabatic transport of electrons by

$$\Delta E = \frac{B_{\text{min}}}{B_{\text{max}}} \frac{\gamma + 1}{2} E, \tag{3}$$

where B_{min} is the minimal magnetic field at the center (the analyzing plane), B_{max} is the maximal magnetic field at the exit of the spectrometer, and γ is the relativistic gamma-factor. The magnetic field configuration of $B_{min} = 2.7 \times 10^{-4}$ T and $B_{max} = 4.2$ T was set up such that an energy resolution of $\Delta E = 1.17$ eV at $E = 17.8$ keV was obtained. With a source magnetic field of $B_S = 2.52$ T, the maximum electron acceptance angle was $\theta_{max} = \arcsin \sqrt{B_S/B_{max}} \approx 51°$ and the accepted forward solid angle fraction was $\Delta\Omega/2\pi \approx 37\%$.

We have measured the zero-energy-loss peak of the K, L_3, and the doublet N_2, N_3 conversion electrons of the 32 keV transition, denoted as K-32, L_3-32, and $N_{2,3}$-32. The K-32 line has an energy of 17.82 keV, which is about 750 eV below the tritium β-spectrum endpoint and can be used for calibrating the spectrometers in tritium β-decay measurements. Its line width is about 2.7 eV [19]. The L_3-32 line with an energy of 30.47 keV has a line width of about 1.2 eV and a ~ 1.5 times higher intensity. In the KATRIN experiment this line is foreseen to be used for space charge investigations in the WGTS. The close doublet $N_{2,3}$-32 has a lower intensity but a natural width that is much smaller than the spectrometer resolution. There are no other strong lines above its energy of 32.14 keV. This is an important feature for an integrating spectrometer since the $N_{2,3}$-32 doublet is superimposed on the intrinsic spectrometer background only. The doublet is essential in studying the MAC-E filter transmission function.

The ^{83m}Kr conversion electron integral energy spectra were obtained by changing the MAC-E filter retarding energy equidistantly in a region around the centroid of each line. The range was about 27 eV for K-32 and 15 eV for L_3-32 and $N_{2,3}$-32. The step size setpoints of 0.5 eV, 0.25 eV and 0.2 eV, respectively, were chosen to reflect the line width and the step size reproducibility of 1 ppm standard deviation relative to the high-voltage value. The acquisition time at each voltage point was uniform for a given line with the values of 60 s for K-32 and L_3-32 and 150 s for $N_{2,3}$-32. Thus, the scanning time of a single spectrum was negligible with respect to the decay constant of the parent ^{83}Rb. For a given high-voltage setting, the count rate was determined for each FPD pixel by summing all detected events in the region -3 keV to 2 keV around the expected electron energy [40], the asymmetry of which accounts for electron energy losses in the FPD dead layer. Integral spectra are obtained by plotting the count rate against the retarding energy. A $\sim$50 Hz high-voltage ripple was present during the measurements[27]. It is a near-sinusoidal signal with amplitudes of 187 mV at -18 kV and 208 mV at -30 kV [47]. The integrated rate of the measured lines over 137 operating detector pixels that have observed the ^{83m}Kr electrons[28] amounted to about 4.1 kcps (K-32), 6.7 kcps (L_3-32), and 0.16 kcps ($N_{2,3}$-32), respectively. Detector dead time is negligible at these low count rates [40]. The total amount of electrons recorded over the whole operating part of the FPD amounted to about 2×10^7, 1×10^7, and 1×10^6, respectively.

4. Analysis

4.1. Electron line shape

A Lorentzian function is used to describe the shape of the conversion electron differential energy distribution:

$$L(E; A, E_0, \Gamma) = \frac{A}{\pi} \frac{\Gamma/2}{(E - E_0)^2 + \Gamma^2/4}. \tag{4}$$

[27] The active regulation system to counteract the high-voltage ripple [40] was not in operation, but is foreseen to be used in future measurements.
[28] Due to a small misalignment of the setup, some FPD pixels were shadowed and could not observe ^{83m}Kr electrons [40].

The parameters are the normalization factor A, the effective line position (centroid) E_0, and the line width (full width at half maximum) Γ. To account for thermal Doppler broadening at the temperature $T = 100$ K, the Lorentzian is convolved with a Gaussian function (normalized to one), yielding a Voigt function V. The Gaussian part is considered to have a centroid of zero and a fixed width of $\sigma = \sqrt{EkT(\gamma + 1)m_e/m_{Kr}}$, where k is the Boltzmann constant, m_e the electron mass, and m_{Kr} the atomic ^{83m}Kr mass. The width σ thus reads 46 meV, 60 meV and 62 meV for K-32, L$_3$-32, and N$_{2,3}$-32, respectively.

To describe the MAC-E filter response to electrons, we consider the relativistic transmission function

$$
T(E, qU) = \begin{cases} 0, & E - qU < 0, \\ \dfrac{1 - \sqrt{1 - \frac{E-qU}{E}\frac{2}{\gamma+1}\frac{B_S}{B_{min}}}}{1 - \sqrt{1 - \frac{B_S}{B_{max}}}}, & 0 \leqslant E - qU \leqslant \Delta E, \\ 1, & E - qU > \Delta E. \end{cases} \tag{5}
$$

In the presence of the high-voltage (HV) ripple described above, each electron experiences a different retarding potential according to the actual phase of the ripple signal. The variation of the potential within the electron transport time is negligible. The observed events include all possible phase values, leading effectively to a broadening of the transmission function. This broadening is taken into account by convolving the transmission function with a digitized oscilloscope waveform of the ripple taken during the measurements. Consequently, the onset of the electron transmission is effectively shifted from qU to a lower value $qU_{min} < qU$. Furthermore, the energy resolution is affected by synchrotron energy loss of the electrons on their way towards the spectrometer. Using the particle-tracking simulation package Kassiopeia [48], it was determined that the energy loss would lead to a degradation in energy resolution of about 30 meV at 18 keV up to 40 meV at 30 keV. Altogether we obtain a more accurate description of the transmission function $T'(E, qU)$ after making the aforementioned corrections.

The conversion electron integral line shape is calculated as

$$
I(qU; A, E_0, \Gamma) = \int_{qU_{min}}^{+\infty} V(E; A, E_0, \Gamma)\, T'(E, qU)\, dE. \tag{6}
$$

Each detector pixel observes a different minimal magnetic field $B_{min,i}$ and retarding potential offset ΔqU_i in the analyzing plane due to residual field inhomogeneities there. These quantities were obtained with Kassiopeia [48].

4.2. K-32 and L$_3$-32 lines

In the maximum likelihood analysis, we have assumed for the K-32 and L$_3$-32 lines that the count rate $r = N/t$ follows the normal distribution and estimated its statistical uncertainty as $\sqrt{N}/t$, where N is the measured number of counts per voltage step and t is the acquisition time. To account for the contributions of the higher-energy ^{83m}Kr lines and the intrinsic spectrometer background, a constant offset C was added to the integral shape in equation (6) such that the fit model was $M = I(qU; A, E_0, \Gamma) + C$. For each pixel, we performed $\chi^2(A, E_0, \Gamma, C)$ function minimization with the four variables as fit parameters. Examples of the integral spectrum from an operating inner pixel and the fit results for the K-32 and L$_3$-32 lines are shown in figure 1. The constant C does not reflect the combined full intensities of the higher-energy lines as can be seen from the K-32 spectrum. The reason is that the higher-energy electrons have high surplus energies with respect to the retarding energy of the spectrometer and are
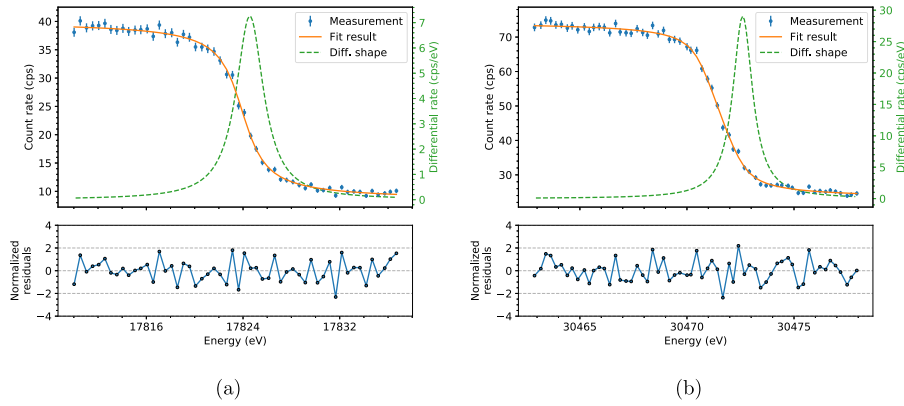
Figure 1. The integral spectra of an operating inner pixel and fit results of the (a) K-32 and (b) L$_3$-32 lines. A negative shift corresponding to the potential offset in the analyzing plane ΔqU was added to the retarding energy qU. The solid curve represents the integral spectrum model in equation (6) with the line shape parameters as obtained from the maximum likelihood analysis. The dashed curve is the corresponding differential Lorentzian shape of the electron line, see equation (4). The lower plots show the residuals of the fit normalized to the statistical uncertainty.

Table 1. The best-fit parameters of the conversion electron lines averaged over individual pixels. The N$_{2,3}$-32 spectrum was fitted using a doublet of δ-functions the positions of which were constrained by the penalty term as described in the text. In this case, no line width is given. The average correlation coefficient of the N$_{2,3}$-32 centroids amounts to 0.98.

Line	Effective position E_0 (eV)	Width Γ (eV)
K-32	$17824.576 \pm 0.005_{\text{stat}} \pm 0.018_{\text{syst}}$	$2.774 \pm 0.011_{\text{stat}} \pm 0.005_{\text{syst}}$
L$_3$-32	$30472.604 \pm 0.003_{\text{stat}} \pm 0.025_{\text{syst}}$	$1.152 \pm 0.007_{\text{stat}} \pm 0.013_{\text{syst}}$
N$_2$-32	$32137.098 \pm 0.016_{\text{stat}} \pm 0.048_{\text{syst}}$	—
N$_3$-32	$32137.758 \pm 0.015_{\text{stat}} \pm 0.048_{\text{syst}}$	—

transported through the spectrometer non-adiabatically. The non-adiabaticity leads to a loss of count rate of the higher-energy lines and thus to a smaller value of the constant C compared to a value that would be expected from the combined intensities. The fit model M describes the observed spectrum without any residual structure. The minimum chi-square per degree of freedom (dof) was $\chi^2_{\text{min}}/\text{dof} = \frac{47.28}{50} = 0.95$ and $\chi^2_{\text{min}}/\text{dof} = \frac{52.15}{57} = 0.92$ with the p-values of 0.58 and 0.66, respectively. The mean effective line position and line width from the results of all pixels, weighted by the reciprocal of squared statistical uncertainties obtained from the fit, are listed in table 1. The observed line positions are compared to the expected ones in section 4.5.

4.3. N$_{2,3}$-32 doublet lines

Since the ^{83m}Kr gas is very dilute, the vacancy left after electron emission from the outermost N shell is expected to be long-lived. Therefore, the natural line width is expected to be very narrow and can be approximated by a δ-function which is obtained in the limit $\Gamma \to 0$. Consequently,
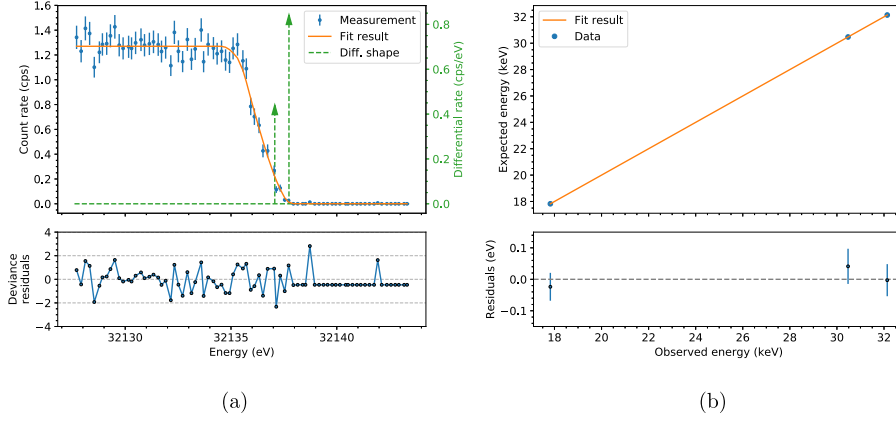
Figure 2. (a) The integral spectrum of an operating pixel and the fit results of the $N_{2,3}$-32 doublet. The differential shape of both lines, for which zero natural width was assumed, is expressed by a δ-function which is depicted here by an arrow. The arrow height corresponds to the normalization factor obtained from the fit. (b) A comparison of the effective and the expected line positions for the K-32, L_3-32, and N_3-32 lines and a straight line fit to the data points assuming a fixed slope of one. The uncertainties shown in the residual plot take into account contributions from both the expected and the effective line positions. The common offset due to the gamma-ray energy uncertainty and the difference of work functions was left as a free parameter.

the observed line shape is dominated by the spectrometer resolution of $\Delta E = 2.13$ eV at 32.1 keV, see equation (3), and the presence of the HV ripple. Thus, in this case, the fit model was based on a doublet of δ-functions with $M = I(qU; A^{\mathrm{II}}, E_0^{\mathrm{II}}) + I(qU; A^{\mathrm{III}}, E_0^{\mathrm{III}}) + C$, where the upper indices II and III refer to N_2-32 and N_3-32, respectively.

Due to the small number of counts at energies above the effective line position, namely about 4.3 counts on average per pixel in all points in the background-only region combined, we have assumed that the observed number of counts follows a Poisson distribution. To break the degeneracy of the doublet parameters, a Gaussian penalty term was introduced into the likelihood function to restrict the difference of the effective line positions $\Delta E_0 = E_0^{\mathrm{III}} - E_0^{\mathrm{II}}$. This difference is well known from optical spectroscopy measurements of electron binding energies to be $\Delta E_0^{\mathrm{best}} \pm \sigma(\Delta E_0) = 0.670(14)$ eV [19]. The negative log-likelihood function is

$$-\ln \mathcal{L}(A^{\mathrm{II}}, E_0^{\mathrm{II}}, A^{\mathrm{III}}, E_0^{\mathrm{III}}, C) + \frac{1}{2}\left(\frac{\Delta E_0 - \Delta E_0^{\mathrm{best}}}{\sigma(\Delta E_0)}\right)^2, \qquad (7)$$

where $\mathcal{L}$ is the likelihood of the parameters in the argument given the observed counts.

An example of the spectrum from an operating inner pixel and the fit result of the doublet are shown in figure 2(a). The fit residuals shown in the plot are defined as res $= \mathrm{sgn}(N - M_t)\sqrt{2\left[N\ln(N/M_t) - (N - M_t)\right]}$ with the model number of counts $M_t = Mt$. We have estimated the *p*-value of the fit by means of a Monte Carlo study: toy measurements were generated from the best-fit model assuming Poisson distribution and corresponding negative log-likelihood function was minimized. From the results of 10^5 trials, the *p*-value was determined to be 0.44. The excellent fit of the doublet supports the eV-scale resolution of the main spectrometer. The effective line positions of the $N_{2,3}$-32 doublet lines averaged over all pixels are listed in table 1.

4.4. Systematic effects

A significant systematic effect to be considered is the readout uncertainty of the HV system at the order of 0.7 ppm to 0.9 ppm in dependence on the line position [47]. Another contribution comes from the uncertainty of the transmission function width that we have estimated to be 1% [49]. It is dominated by the uncertainties of the electric and magnetic field values in the analyzing plane and, to a lesser degree, by the variations in the path length of the electrons on their way through the source section, leading to different synchrotron energy losses. We have also considered a conservative 20% uncertainty of the HV ripple [47] experienced by the electrons at the analyzing plane. The WGTS temperature and magnetic field stability were both one order of magnitude better than the design requirements [40] and are negligible. The combined systematic uncertainty of the effective line position and width from the considered contributions is listed in table 1. The differences between the measured line positions can be used for a detailed cross-check of the high-voltage system calibration. The results of this investigation are discussed in a separate paper [47].

4.5. Expected and observed line position

In order to relate the effective line position from table 1 to the one expected from equation (1), the difference of the source and spectrometer work functions, which was not determined beforehand, would have to be taken into account, see equation (2). In addition, the expected line position is subject to a large systematic uncertainty of the 32-keV gamma-ray energy of 0.5 eV [19]. The work-function difference and inaccuracy due to the gamma-ray energy uncertainty can contribute to a small constant shift between the expected and the effective line position. Following the equations (1) and (2), this shift is the same for all lines of the 32 keV transition when taking into account the line-dependent electron binding energies $E_{e,bin}$ and recoil energies $E_{e,rec}$. Therefore, the expected and observed line positions can be compared while leaving the common offset free.

The expected line position is compared to the observed one in figure 2(b). The statistical and systematic uncertainties of the observed line positions from table 1 were added in quadrature. The uncertainties of the expected line positions come from the uncertainties of the electron binding energies which are at the order of a few tens of meV [19]. Assuming a linear function with a fixed slope of one, the combined uncertainties showed in the residual plot of figure 2(b) were obtained by adding the observed and expected line position uncertainties in quadrature. The plot demonstrates the linearity of the KATRIN energy scale and the consistency of the N_3-32 effective line position from the doublet analysis of the $N_{2,3}$-32 region. The uncertainty introduced due the common offset has no impact on the systematic uncertainty of the observed line width.

5. Conclusion

In summary, we have obtained high-resolution integral spectra of the ^{83m}Kr conversion electron lines with the KATRIN main spectrometer. The spectra were analyzed by means of maximum likelihood analysis taking into account the relevant systematic effects, such as Doppler broadening, high-voltage ripple, synchrotron energy loss, and uncertainties of the electric and magnetic fields in the analyzing plane. The results demonstrate the integrity of the KATRIN beamline, an as-designed large angular acceptance and high energy resolution of the KATRIN main spectrometer, good energy linearity over a range of 14 keV and understanding of the observed spectra and hence the KATRIN apparatus. In a future measurement, a complete KATRIN setup including also the gold-plated rear wall, ^{83m}Kr circulating in the WGTS and

active regulation of the high-voltage system will be applied. The active regulation of the HV system will further improve the KATRIN energy resolution.

Acknowledgments

ORCID iDs

M Slezák ⓘ https://orcid.org/0000-0003-4289-7816

References

[1] Cleveland B T, Daily T, Davis R Jr, Distel J R, Lande K, Lee C K, Wildenhain P S and Ullman J 1998 *Astrophys. J.* **496** 505–26
[2] Fukuda Y *et al* Super-Kamiokande Collaboration 1998 *Phys. Rev. Lett.* **81** 1562–7
[3] Ahmad Q R *et al* SNO Collaboration 2002 *Phys. Rev. Lett.* **89** 011301
[4] Bennett C L *et al* WMAP Collaboration 2013 *Astrophys. J. Suppl.* S **208** 20
[5] Ade P A R *et al* Planck Collaboration 2016 *Astron. Astrophys.* **594** A13
[6] Agostini M *et al* GERDA Collaboration 2017 *Nature* **544** 47–52
[7] Gando A *et al* KamLAND-Zen Collaboration 2016 *Phys. Rev. Lett.* **117** 082503
[8] Albert J B *et al* EXO-200 Collaboration 2014 *Nature* **510** 229–34
[9] Angrik J *et al* KATRIN collaboration 2005 *FZKA Scientific Report 7090* http://bibliothek.fzk.de/zb/berichte/FZKA7090.pdf
[10] Formaggio J A *et al* Project 8 Collaboration 2012 *J. Phys. Conf. Ser.* **375** 042005
[11] Gastaldo L *et al* 2017 *Eur. Phys. J.-Spec. Top.* **226** 1623–94
[12] Alpert B *et al* 2015 *Eur. Phys. J.* C **75** 112
[13] Fermi E 1934 *Z. Phys.* **88** 161–77
[14] Otten E W and Weinheimer C 2008 *Rep. Prog. Phys.* **71** 086201
[15] Kraus C *et al* 2005 *Eur. Phys. J.* C **40** 447–68
[16] Aseev V N *et al* 2011 *Phys. Rev.* D **84** 112003
[17] Aker M *et al* KATRIN Collaboration 2019 *Phys. Rev. Lett.* **123** 221802
[18] McCutchan E A 2015 *Nucl. Data Sheets* **125** 201
[19] Vénos D, Sentkerestiová J, Dragoun O, Slezák M, Ryšavý M and Špalek A 2018 *J. Instrum.* **13** T02012
[20] Robertson R G H, Bowles T J, Stephenson G J, Wark D L, Wilkerson J F and Knapp D A 1991 *Phys. Rev. Lett.* **67** 957–60
[21] Picard A *et al* 1992 *Nucl. Instrum. Meth.* B **63** 345–58
[22] Stoeffl W and Decman D J 1995 *Phys. Rev. Lett.* **75** 3237–40
[23] Decamp D *et al* ALEPH Collaboration 1990 *Nucl. Instrum. Meth.* A **294** 121–78
[24] Acharya S *et al* ALICE Collaboration 2017 *Nucl. Instrum. Meth.* A **881** 88–127
[25] Chan A *et al* 1995 *IEEE Trans. Nucl. Sci.* **42** 491
[26] Afanasiev S *et al* 1999 *Nucl. Instrum. Meth.* A **430** 210–44
[27] Kastens L W, Cahn S B, Manzur A and McKinsey D N 2009 *Phys. Rev.* C **80** 045809
[28] Lippincott W H, Cahn S B, Gastler D, Kastens L W, Kearns E, McKinsey D N and Nikkel J A 2010 *Phys. Rev.* C **81** 045803

[29] Aprile E *et al* XENON Collaboration 2017 *Eur. Phys. J.* C **77** 881
[30] Akerib D S *et al* LUX Collaboration 2018 *J. Instrum.* **13** P02001
[31] Aalseth C E *et al* 2018 *Eur. Phys. J. Plus* **133** 131
[32] Rosendahl S *et al* 2014 *J. Instrum.* **9** P10010
[33] Asner D M *et al* Project 8 Collaboration 2015 *Phys. Rev. Lett.* **114** 162501
[34] Ashtari Esfahani A *et al* Project 8 Collaboration 2017 *J. Phys.* G **44** 054004
[35] Ostrick B 2008 Eine kondensierte ^{83m}Kr-Kalibrationsquelle für das KATRIN-experiment *PhD Thesis* University of Münster http://repositorium.uni-muenster.de/document/miami/606200b4-7e48-49b7-8a5a-87d51948111b/diss_ostrick.pdf
[36] Picard A *et al* 1992 *Z. Phys.* A **342** 71–8
[37] Campbell J L and Papp T 2001 *At. Data Nucl. Data Tables* **77** 1–56
[38] Lobashev V M and Spivak P E 1985 *Nucl. Instrum. Meth.* A **240** 305–10
[39] Bornschein B 2006 *Prog. Part. Nucl. Phys.* **57** 38–48
[40] Arenz M *et al* KATRIN Collaboration 2018 *J. Instrum.* **13** P04020
[41] Gil W, Bonn J, Bornschein B, Gehring R, Kazachenko O, Kleinfeller J and Putselyk S 2010 *IEEE Trans. Appl. Supercond.* **20** 316–9
[42] Amsbaugh J F *et al* 2015 *Nucl. Instrum. Meth.* A **778** 40–60
[43] Vénos D, Špalek A, Lebeda O and Fišer M 2005 *Appl. Radiat. Isot.* **63** 323–7
[44] Sentkerestiová J, Dragoun O, Lebeda O, Ryšavý M, Sturm M and Vénos D 2018 *J. Instrum.* **13** P04018
[45] Kuckert L 2016 The windowless gaseous tritium source of the KATRIN Experiment –Characterisation of gas dynamical and plasma properties *PhD Thesis* (Karlsruhe Institute of Technology) http://nbn-resolving.org/urn:nbn:de:swb:90-650776
[46] Belesev A I *et al* 2008 *Phys. Atom. Nucl.* **71** 427–36
[47] Arenz M *et al* KATRIN Collaboration 2018 *Eur. Phys. J.* C **78** 368
[48] Furse D *et al* 2017 *New J. Phys.* **19** 053012
[49] Erhard M 2016 Influence of the magnetic field on the transmission characteristics and neutrino mass systematic of the KATRIN experiment *PhD Thesis* (Karlsruhe Institute of Technology) http://nbn-resolving.org/urn:nbn:de:swb:90-650034